APL Materials

Molecular beam epitaxy of Cd_3As_2 on a III-V substrate

Cite as: APL Mater. 4, 126110 (2016); https://doi.org/10.1063/1.4972999
Submitted: 05 October 2016 • Accepted: 15 November 2016 • Published Online: 23 December 2016

Timo Schumann, Manik Goyal, Honggyu Kim, et al.

Molecular beam epitaxy of Cd_3As_2 on a III-V substrate

Timo Schumann,[a] Manik Goyal, Honggyu Kim, and Susanne Stemmer[b]
Materials Department, University of California, Santa Barbara, California 93106-5050, USA

(Received 5 October 2016; accepted 15 November 2016; published online 23 December 2016)

Epitaxial, strain-engineered Dirac semimetal heterostructures promise tuning of the unique properties of these materials. In this study, we investigate the growth of thin films of the recently discovered Dirac semimetal Cd_3As_2 by molecular beam epitaxy. We show that epitaxial Cd_3As_2 layers can be grown at low temperatures (110 °C–220 °C), *in situ*, on (111) GaSb buffer layers deposited on (111) GaAs substrates. The orientation relationship is described by $(112)_{Cd_3As_2} \parallel (111)$ GaSb and $[1\bar{1}0]_{Cd_3As_2} \parallel [\bar{1}01]_{GaSb}$. The films are shown to grow in the low-temperature, vacancy ordered, tetragonal Dirac semimetal phase. They exhibit high room temperature mobilities of up to 19 300 cm^2/Vs, despite a three-dimensional surface morphology indicative of island growth and the presence of twin variants. The results indicate that epitaxial growth on more closely lattice matched buffer layers, such as InGaSb or InAlSb, which allow for imposing different degrees of epitaxial coherency strains, should be possible. [http://dx.doi.org/10.1063/1.4972999]

Topological semimetals are a newly discovered class of materials that have gathered significant attention due to their unique properties. For example, bulk single crystals of these materials show extremely high electron mobilities, negative and linear magnetoresistance,[1–4] and surface Fermi arcs.[5] Dirac semimetals are characterized by a linearly dispersive band crossing close to the Fermi energy ("Dirac nodes"). They can potentially be tuned between different topological phases, such as Weyl semimetals, topological superconductors, and topological insulators.[6] Cd_3As_2, long known for its very high electron mobility,[7] was recently recognized as a Dirac semimetal.[8] It has a pair of Dirac nodes that can be observed in x-ray photoemission experiments.[9,10]

Cd_3As_2 thin films are required for integration into devices and for the engineering of topological phases, using heterostructure approaches such as epitaxial strain, field effect, or quantum confinement.[11] Epitaxial films are also desirable to reduce extended defects. Previous studies of Cd_3As_2 films have used amorphous substrates (e.g., SiO_2, fused quartz, and borosilicate),[12–14] substrates with the rocksalt crystal structure (NaCl and KCl),[15,16] or weakly bonding substrates (mica).[15,17,18] None of these substrates are expected to facilitate epitaxial growth and no information about film textures was given. Furthermore, the carrier mobilities of these films have remained below those reported for bulk single crystals.

The Dirac semimetal phase of Cd_3As_2 is tetragonal and belongs to the $I4_1/acd$ space group with lattice parameters a = 12.633 Å and c = 25.427 Å.[19] Its preferred growth surface is the (112).[20,21] The atom arrangements near the (112) growth plane can be compared with those in the (111) planes of III-V semiconductors with the cubic zincblende structure, such as GaAs or GaSb, as shown in Fig. 1. The two surfaces show similar hexagonal arrangements of their group V elements that should promote an epitaxial relationship. The spacing of the group V elements around the hexagon in the (112) plane is 4.4–4.6 Å in Cd_3As_2 vs. 4.3 Å in (111) GaSb. Closer lattice matching can be achieved with ternary III-V alloys, such as $(Ga_xIn_{1-x})Sb$ or $(Al_xIn_{1-x})Sb$. By far the most common growth plane for III-V layers is (001) and few reports exist of smooth, strain-relaxed (111)

[a]Electronic mail: schumann.timo@gmx.net
[b]Electronic mail: stemmer@mrl.ucsb.edu

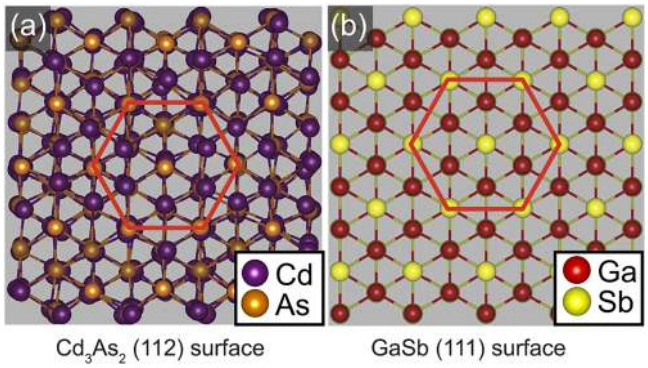

FIG. 1. Atom arrangements about (a) the (112) surface of Cd_3As_2 and (b) the (111) GaSb surface, respectively. The hexagonal arrangement of the group V atoms is indicated by the red lines.

epitaxial III-V layers.[22–24] Here, we investigate if Cd_3As_2 films can be grown epitaxially on (111) GaSb/GaAs substrates using molecular beam epitaxy (MBE). GaSb buffer layers were grown *in situ* by MBE on GaAs(111)A substrates, to reduce the lattice mismatch with the Cd_3As_2 film (~5% vs. ~10% mismatch with GaSb and GaAs, respectively). Furthermore, unlike GaSb substrates, GaAs is electrically insulating, which facilitates the interpretation of electrical measurements at room temperature.

GaAs(111)A (Ga-polar) substrates were cleaned with solvents and etched for 5 min in concentrated HCl prior to loading them into the MBE chamber to remove the native oxide. The substrates were annealed to 200 °C to desorb residual moisture and contaminants before the transfer to the growth chamber, where they were annealed under Sb flux to remove any remaining oxide. Subsequently, GaSb buffer layers were grown at a substrate temperature of 500 °C for 20 min with an Sb beam equivalent pressure (BEP) of 2.5×10^{-7} Torr and a V/III ratio of about 7. Sb was supplied from a cracker cell. The sample was cooled down under Sb_2 flux, which was terminated at 350 °C, to the substrate temperature for Cd_3As_2 growth. Cd_3As_2 was evaporated from solid pieces, using an effusion cell with the BEP fluxes varying between 2×10^{-7} and 5×10^{-6} Torr. 100–300 nm thick films were grown at substrate temperatures between 110 °C and 220 °C for 60 min. Further increases in substrate temperature at these flux rates resulted in no growth. Film growth and microstructures were monitored *in situ* with reflection high-energy electron diffraction (RHEED) and studied *ex situ* using high-resolution x-ray diffraction (XRD), atomic force microscopy (AFM), and scanning transmission electron microscopy (STEM). The sheet carrier concentration and carrier mobility were determined using Hall and sheet resistance measurements in the Van der Pauw geometry. The film surface oxidizes upon air exposure but no further degradation was observed during/after processing and electrical measurement.

RHEED along $\langle 1\bar{1}0 \rangle$ of the zincblende substrate after the growth of Cd_3As_2 films at different substrate temperatures is shown in Figs. 2(a)–2(e). Films grown at lower substrate temperatures (110 °C and 140 °C) showed spotty RHEED patterns, indicative of a three-dimensional surface. Growth at higher substrate temperatures (>170 °C) resulted in a streaky RHEED pattern, which indicated smooth films on the length scale probed by RHEED. The corresponding 10×10 μm^2 AFM images of the respective samples are shown in Figs. 2(f)–2(j). The GaSb buffer was very smooth, albeit with some step bunching [Fig. 2(f)], with a root mean square roughness of 1.3 nm, comparable to optimized (111) III-V layers reported in the literature.[22] In contrast, the Cd_3As_2 film surfaces were significantly rougher and showed triangular shaped islands whose average diameter increased from ~50 nm (110 °C) to ~3 μm (210 °C), indicating three-dimensional growth despite the islands having flat surfaces that dominate the RHEED pattern.

Out-of-plane XRD scans of a Cd_3As_2 film are displayed in Figs. 3(a) and 3(b). Peaks from the $\{111\}$ planes of the GaAs substrate and GaSb buffer layer are marked with squares and circles, respectively. Peaks arising from $\{112\}$ planes of the Cd_3As_2 are indicated by triangles. No additional peaks are present, indicating single-phase GaSb and Cd_3As_2 films with a high degree of alignment in the out-of-plane direction. A scan with higher resolution around the Cd_3As_2 224 reflection is shown

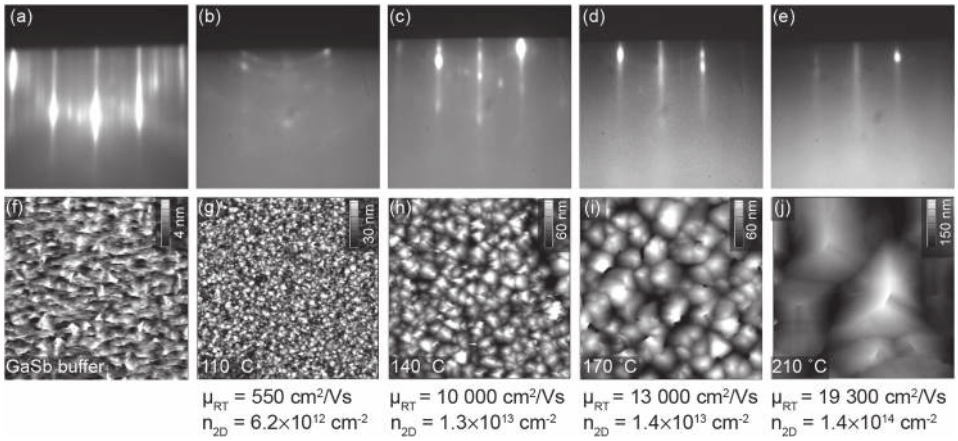

FIG. 2. (a)-(e) RHEED patterns taken along $\langle 1\bar{1}0\rangle_{GaSb}$ of the GaSb buffer layer (a) and after the Cd_3As_2 growth at different substrate temperatures (b)-(e). (f)-(j) Corresponding $10 \times 10\ \mu m^2$ atomic force micrographs. The Hall mobilities and sheet carrier densities measured at 300 K are given underneath each image.

in Fig. 3(b). The observed peak positions agree with those derived from the bulk lattice parameters, indicated by the dotted lines. The observed alignment, $\{112\}_{Cd_3As_2} \parallel \{111\}_{GaSb}$ is a necessary but insufficient criterion for epitaxial growth, in particular since the $\{112\}$ planes are the preferred surface facets of Cd_3As_2. To determine the in-plane alignment between film, buffer layer, and substrate, XRD pole figures were recorded using the Cd_3As_2 4 4 16 [GaAs/GaSb 224] reflections, shown in Fig. 3(c). The film and substrate peaks show the expected threefold symmetry and the peaks are aligned. Cd_3As_2 exhibits a second set of reflections, rotated by 60°, which indicates twinning. To get a more quantitative measure, azimuthal scans of the GaSb 224 and Cd_3As_2 4 4 16 reflections are presented in Fig. 3(d). No twins are detectable in the GaSb buffer layer. The fraction of twinned domains in the Cd_3As_2 film amounts to ~2.5%. The use of miscut substrates should help eliminate twinning.[25] We note that Cd_3As_2 diffraction peaks such as 4 4 16, 8 4 8, and 4 8 8 cannot be distinguished due to the similarity of a and $c/2$ lattice parameters. Therefore, the possibility of additional twinning cannot be eliminated.

To gain further insight into the Cd_3As_2 film structure, Fig. 4 shows high-angle annular dark-field (HAADF) STEM images. The overview image [Fig. 4(a)] shows sharp interfaces without intermixing. Three different polymorphs of Cd_3As_2 have been reported.[21] The low-temperature Dirac semimetal can be described as containing ordered Cd vacancies,[21] in contrast to the high temperature $Fm\bar{3}m$ cubic phase. An intermediate-temperature structure with $P4_2/nm$ symmetry has also been found.[21] As shown in Figs. 4(b)–4(d), STEM allows us to determine the specific phase of the MBE films. A schematic of the structure (I_4/acd space group) viewed along $[1\bar{1}0]_{Cd_3As_2}$ is shown in Fig. 4(b). Focusing on the two rows indicated by red and blue arrows, respectively, we see that in the row marked by red arrows all Cd columns are fully occupied along the viewing direction, while in the next row (blue arrows) only half of the columns are fully occupied with Cd atoms (the dashed circles indicate columns with missing Cd). The columns with missing Cd atoms can be identified in the HAADF-STEM image [Fig. 4(c)] where half of the triplets show a reduced intensity in the row indicated by the blue arrow. Intensity line scans along two rows confirm this, see Fig. 4(d). Since this ordering is specific to the I_4/acd phase, the films grew in the desired Dirac semimetal phase.

An important benchmark for material quality is the charge carrier mobility, which is indicated for the films grown at different substrate temperatures in Fig. 2, along with their sheet carrier densities. All films show n-type conductivity, with room temperature carrier mobilities increasing with substrate temperature from ~550 cm^2/V s to 19 300 cm^2/V s. The latter are comparable to room temperature single crystal values[26] and higher than those for thin films reported in the literature, which were in the range of 2000 cm^2/V s–11 000 cm^2/V s.[13,17,18,27] The GaSb films exhibited sheet resistances that were at least three orders of magnitude higher than those of the Cd_3As_2 films,

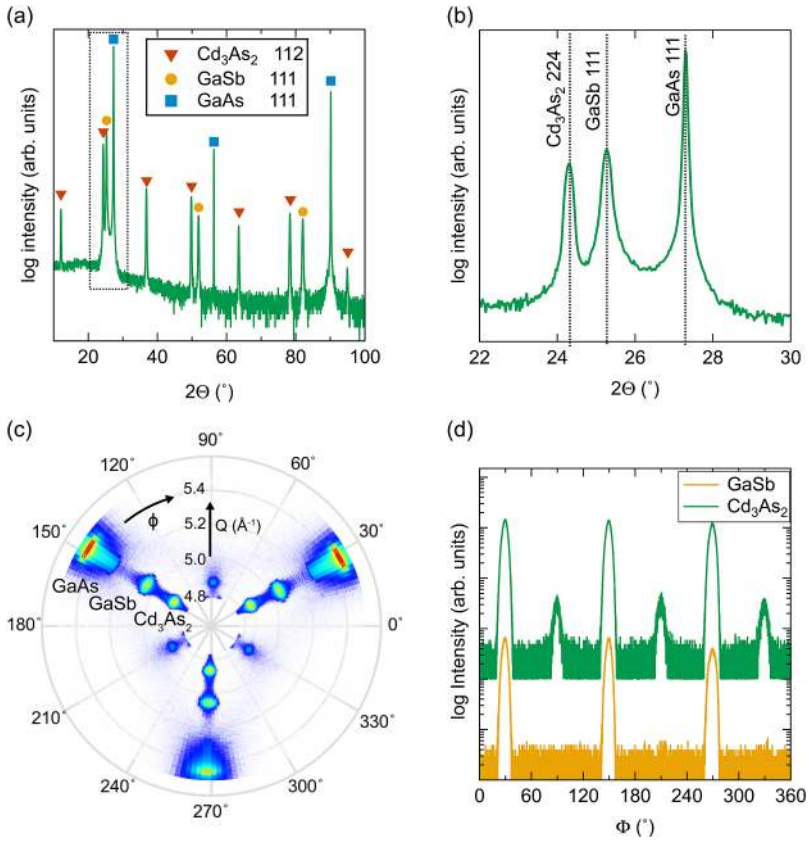

FIG. 3. (a) Out-of-plane XRD of a Cd_3As_2/GaSb/GaAs(111A) sample grown at a substrate temperature of 180 °C. The symbols indicate the family of peaks from each material. A higher resolution scan of the region indicated by the dashed box is given in (b). The dotted lines indicate the expected peak positions calculated from the bulk lattice parameters. (c) In-plane pole figure around the GaAs/GaSb 224 and Cd_3As_2 4 4 16 reflections, showing the in-plane alignment between the substrate, buffer layer, and film. (d) Line scans of the GaSb and Cd_3As_2 peaks shown in (c).

ensuring that the measurements were dominated by the properties of the Cd_3As_2 films. Investigations of the temperature-dependent transport properties, which are complicated, will be the subject of future studies.

To summarize, we have shown that epitaxial Cd_3As_2 thin films that have the crystal structure of the Dirac semimetal phase can be grown by MBE on III-V layers. The high room temperature mobilities of the films are surprising, given their three-dimensional growth morphologies and twinned microstructure, and may indicate some degree of topological protection. Future work should address reducing defect densities. The epitaxial alignment between the film, buffer layer, and substrates indicates routes to further improvements in the films' quality. In particular, larger miscuts can be used to eliminate twinning and better lattice matching can be obtained using InGaSb or InAlSb buffer layers. This will require the development of strain-relaxed, (111)-oriented films of these alloys, which, in contrast to (001) oriented layers, has not yet been extensively studied. Better lattice matching may also improve the growth mode of the Cd_3As_2 layers towards more two-dimensional growth. In addition to further improving materials quality and mobility, the combination of lattice-matched III-V layers and Cd_3As_2 layers will enable the use of heterostructure engineering methods to control the electronic states of this three-dimensional Dirac semimetal.

The authors gratefully acknowledge support through the Vannevar Bush Faculty Fellowship program by the U.S. Department of Defense (Grant No. N00014-16-1-2814). Partial funding was also provided by the U.S. National Science Foundation (Award No. 1125017) and by Northrop Grumman.

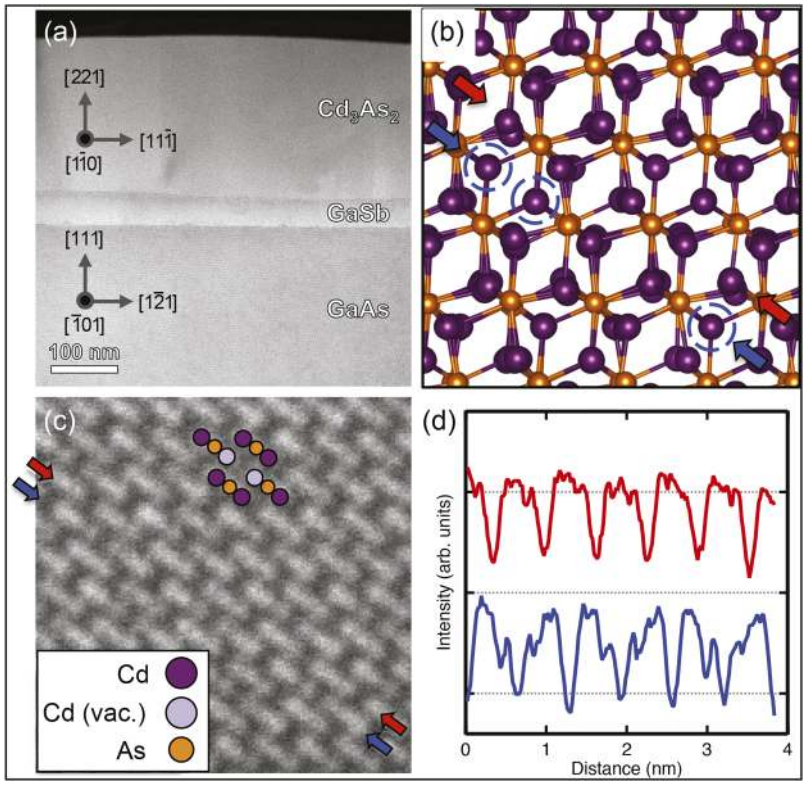

FIG. 4. (a) Low-magnification HAADF-STEM image of a GaAs/GaSb/Cd_3As_2 heterostructure grown at a substrate temperature of 200 °C. (b) Schematic of the structure of Cd_3As_2 in the low temperature $I4_1/acd$ phase projected along [1$\bar{1}$0]. The red and blue arrows mark two inequivalent planes and the circles indicate the positions of columns containing Cd vacancies (see text for details). (c) High resolution HAADF-STEM image along [1$\bar{1}$0] with the corresponding rows indicated by arrows. (d) Intensity profiles (shifted for clarity) obtained from scans along the rows marked in (c). The dips in intensity (corresponding to the Cd vacancies) are clearly visible in the second (blue) curve.

[1] T. Liang, Q. Gibson, M. N. Ali, M. H. Liu, R. J. Cava, and N. P. Ong, "Ultrahigh mobility and giant magnetoresistance in the dirac semimetal Cd_3As_2," Nat. Mater. **14**, 280–284 (2015).
[2] X. Huang, L. Zhao, Y. Long, P. Wang, D. Chen, Z. Yang, H. Liang, M. Xue, H. Weng, Z. Fang, X. Dai, and G. Chen, "Observation of the chiral-anomaly-induced negative magnetoresistance in 3D Weyl semimetal TaAs," Phys. Rev. X **5**, 031023 (2015).
[3] X. L. Wang, Y. Du, S. X. Dou, and C. Zhang, "Room temperature giant and linear magnetoresistance in topological insulator Bi_2Te_3 nanosheets," Phys. Rev. Lett. **108**, 266806 (2012).
[4] H. Li, H. T. He, H. Z. Lu, H. C. Zhang, H. C. Liu, R. Ma, Z. Y. Fan, S. Q. Shen, and J. N. Wang, "Negative magnetoresistance in Dirac semimetal Cd_3As_2," Nat. Commun. **7**, 10301 (2016).
[5] S.-Y. Xu, C. Liu, S. K. Kushwaha, R. Sankar, J. W. Krizan, I. Belopolski, M. Neupane, G. Bian, N. Alidoust, T.-R. Chang, H.-T. Jeng, C.-Y. Huang, W.-F. Tsai, H. Lin, P. P. Shibayev, F.-C. Chou, R. J. Cava, and M. Z. Hasan, "Observation of Fermi arc surface states in a topological metal," Science **347**, 294–298 (2015).
[6] Z. K. Liu, B. Zhou, Y. Zhang, Z. J. Wang, H. M. Weng, D. Prabhakaran, S. K. Mo, Z. X. Shen, Z. Fang, X. Dai, Z. Hussain, and Y. L. Chen, "Discovery of a three-dimensional topological Dirac semimetal, Na_3Bi," Science **343**, 864–867 (2014).
[7] A. J. Rosenberg and T. C. Harman, "Cd_3As_2—A noncubic semiconductor with unusually high electron mobility," J. Appl. Phys. **30**, 1621–1622 (1959).
[8] Z. J. Wang, H. M. Weng, Q. S. Wu, X. Dai, and Z. Fang, "Three-dimensional Dirac semimetal and quantum transport in Cd_3As_2," Phys. Rev. B **88**, 125427 (2013).
[9] S. Borisenko, Q. Gibson, D. Evtushinsky, V. Zabolotnyy, B. Buchner, and R. J. Cava, "Experimental realization of a three-dimensional Dirac semimetal," Phys. Rev. Lett. **113**, 165109 (2014).
[10] M. Neupane, S. Y. Xu, R. Sankar, N. Alidoust, G. Bian, C. Liu, I. Belopolski, T. R. Chang, H. T. Jeng, H. Lin, A. Bansil, F. Chou, and M. Z. Hasan, "Observation of a three-dimensional topological Dirac semimetal phase in high-mobility Cd_3As_2," Nat. Commun. **5**, 3786 (2014).
[11] H. Pan, M. M. Wu, Y. Liu, and S. A. Yang, "Electric control of topological phase transitions in Dirac semimetal thin films," Sci. Rep. **5**, 14639 (2015).
[12] H. Matsunami and T. Tanaka, "Cd_3As_2 thin film magnetoresistor," Jpn. J. Appl. Phys., Part 1 **10**, 600–603 (1971).
[13] J. J. Dubowski and D. F. Williams, "Growth and properties of Cd_3As_2 films prepared by pulsed-laser evaporation," Can. J. Phys. **63**, 815–818 (1985).

[14] M. Din and R. D. Gould, "Van der Pauw resistivity measurements on evaporated thin films of cadmium arsenide, Cd_3As_2," Appl. Surf. Sci. **252**, 5508–5511 (2006).
[15] L. Zdanowicz, S. Miotkowska, and M. Niedzwiedz, "Structure, growth and crystallization effects in thin films of cadmium arsenide," Thin Solid Films **34**, 41–45 (1976).
[16] J. Jurusik and L. Zdanowicz, "Electron microscope investigations of the growth morphology of cadmium arsenide films vacuum deposited at various substrate temperatures," Thin Solid Films **67**, 285–291 (1980).
[17] Y. Liu, C. Zhang, X. Yuan, T. Lei, C. Wang, D. D. Sante, A. Narayan, L. He, S. Picozzi, S. Sanvito, R. Che, and F. Xiu, "Gate-tunable quantum oscillations in ambipolar Cd_3As_2 thin films," NPG Asia Mater. **7**, e221 (2015).
[18] P. Cheng, C. Zhang, Y. Liu, X. Yuan, F. Song, Q. Sun, P. Zhou, D. W. Zhang, and F. Xiu, "Thickness-dependent quantum oscillations in Cd_3As_2 thin films," New J. Phys. **18**, 083003 (2016).
[19] G. A. Steigmann and J. Goodyear, "The crystal structure of Cd_3As_2," Acta Crystallogr., Sect. B: Struct. Crystallogr. Cryst. Chem. **B24**, 1062–1067 (1968).
[20] L. P. He, X. C. Hong, J. K. Dong, J. Pan, Z. Zhang, J. Zhang, and S. Y. Li, "Quantum transport evidence for the three-dimensional Dirac semimetal phase in Cd_3As_2," Phys. Rev. Lett. **113**, 246402 (2014).
[21] M. N. Ali, Q. Gibson, S. Jeon, B. B. Zhou, A. Yazdani, and R. J. Cava, "The crystal and electronic structures of Cd_3As_2, the three-dimensional electronic analogue of graphene," Inorg. Chem. **53**, 4062–4067 (2014).
[22] E. Hall and H. Kroemer, "Surface morphology of GaSb grown on (111)B GaAs by molecular beam epitaxy," J. Cryst. Growth **203**, 297–301 (1999).
[23] R. X. Yang, Y. B. Wu, C. L. Niu, and F. Yang, "Growth control of GaAs epilayers with specular surface on nonmisoriented (111)B substrates by MBE," ECS Trans. **27**, 351–357 (2010).
[24] T. Hayakawa, M. Kondo, T. Suyama, K. Takahashi, S. Yamamoto, and T. Hijikata, "Reduction in threshold current density of quantum well lasers grown by molecular beam epitaxy on 0.5° misoriented (111)B substrates," Jpn. J. Appl. Phys., Part 2 **26**, L302–L305 (1987).
[25] M. C. Debnath, T. D. Mishima, M. B. Santos, L. C. Phinney, T. D. Golding, and K. Hossain, "High electron mobility in InSb epilayers and quantum wells grown with AlSb nucleation on Ge-on-insulator substrates," J. Vac. Sci. Technol., B: Nanotechnol. Microelectron.: Mater., Process., Meas., Phenom. **32**, 02C116 (2014).
[26] W. Zdanowicz and L. Zdanowicz, "Semiconducting compounds of the AII BV group," Annu. Rev. Mater. Sci. **5**, 301–328 (1975).
[27] B. Zhao, P. H. Cheng, H. Y. Pan, S. Zhang, B. G. Wang, G. H. Wang, F. X. Xiu, and F. Q. Song, "Weak antilocalization in Cd_3As_2 thin films," Sci. Rep. **6**, 22377 (2016).